

Measurement of smoke concentration using degenerate four-wave mixing

T C Cole¹, W A Cole¹, T M Brown² and R W Pitz

Department of Mechanical Engineering, Vanderbilt University, Nashville, TN 37235, USA

E-mail: warrencole@naxs.net, tom.brown@msfc.nasa.gov and robert.w.pitz@vanderbilt.edu

Received 17 August 2001, in final form 4 December 2001, accepted for publication 7 December 2001

Published 28 February 2002

Online at stacks.iop.org/MST/13/464

Abstract

Degenerate four-wave mixing (DFWM) was successfully used to monitor a wide range of smoke concentrations ($0.1\text{--}10\text{ mg m}^{-3}$) in sample cells. To the authors' knowledge, this is the first measurement of smoke by DFWM. The DFWM method is very sensitive, measuring down to ~ 0.1 ppb soot volume fraction. To verify the visible laser DFWM system, NO_2 concentrations from 2 to 200 ppm were measured with a sensitivity of 2 ppm of NO_2 . Both smoke and NO_2 species were resonantly pumped at 500 nm by an excimer-pumped dye laser (~ 2 mJ/pulse). The DFWM signal from both NO_2 and smoke showed a squared dependence on concentration. Single-pulse measurements of NO_2 and smoke in sample cells indicate that temporally and spatially resolved *in situ* DFWM measurements are feasible for engine exhausts.

Keywords: soot measurement, smoke emissions, engine exhausts, pollution measurement, degenerate four-wave mixing, particulate matter

1. Introduction

Smoke exhaust from jet, gasoline and diesel engines has long been recognized as an environmental and health hazard [1]. Recently, smoke exhaust has come under scrutiny due to the increased health concerns associated with small particulates below $10\text{ }\mu\text{m}$ diameter [2].

Sampling of smoke in jet engine exhausts is problematic due to the need to measure low concentrations in an environment of high ambient noise (up to 160 dB near a jet engine), vibration and dirt. In the United States, the accepted method for determining smoke emissions from jet engines is by filter sampling [3, 4]. However, filter sampling suffers from losses of soot particles via coating on the walls of the sample line. Also, modern jet engines produce extremely small amounts of smoke (less than 2 mg m^{-3}) and filtering methods have insufficient sensitivity. Whereas real-time smoke emission measurement is desired to provide more rapid characterization of smoke emissions from new jet engines, the results of filter measurements are not available until the

engine testing is complete. For combustor component and sector testing, information is needed on spatial distribution and fluctuations of soot concentration. This type of knowledge requires a nonintrusive method that has both excellent temporal and spatial resolution. Thus, there remains a need of real-time, accurate, sensitive, *in situ* measurement of smoke from jet engine exhaust.

Optical methods have been developed to measure smoke in engine exhausts. Smoke measurements have been made using photoacoustic and photothermal deflection methods. Photoacoustic methods measuring diesel smoke require long sample lines to isolate the microphone from the noisy diesel engine [5, 6]. Photothermal deflection measurements, where the smoke concentration is related to the angular deflection of a CW probe beam, have been accomplished in sample cells [7, 8] and in flames [9]. However, *in situ* measurements of smoke in engine exhausts using photothermal deflection will be difficult. CW probe beam deflections due to thermal heating by the pump beam are difficult to differentiate from deflections due to thermal gradients in the engine exhaust.

Laser-induced incandescence (LII) has been extensively applied to measure soot concentration in flames. LII of soot was first studied as interference to Raman scattering

¹ Present address: 502 Biltmore Avenue, Lynchburg, VA 24502, USA.

² Present address: NASA Marshall Space Flight Center, Huntsville, AL 35812, USA.

measurements by Eckbreth [10] and later proposed as a soot measurement technique by Melton [11]. In the first application, Dec and co-workers applied LII to image soot concentrations in diesel engines [12, 13]. Subsequently, the method has been developed and applied by a number of researchers to measure soot in flames [14–16]. To date, all the LII measurements of soot volume fraction in flames have been in the range of 0.1–20 ppm [17, 18]. Modern jet engine exhausts have smoke numbers of 10–20, that translate to soot concentrations of 1–2 mg m⁻³ and soot volume fractions of 1–2 ppb [19]. These levels of soot volume fraction are about 1000 times lower than the values previously measured by the LII method in flames. Recently, more sensitive LII measurements have been made detecting soot down to 2.2 mg m⁻³ concentration in diesel exhausts [20] and down to ~0.01 mg m⁻³ concentration in heated air jets [21]. When recently applied to jet engine exhausts, the LII method only gave qualitative measurements of soot concentration due to problems imaging the soot incandescence across the large exhaust plume [22].

Degenerate four-wave mixing (DFWM) is a laser diagnostic technique that is capable of making very sensitive measurements at a point and produces a signal that is a coherent laser beam that can be detected far from the measurement location. In contrast, the signal emission from LII spreads isotropically in space making detection at a distance difficult. In DFWM, two laser ‘pump’ beams interact with a third ‘probe’ beam in a crossing zone to form a new coherent beam, which contains information regarding the nature of the media in which it is produced. Because the spatial resolution is limited only by the size of the beam crossing zone, DFWM offers excellent spatial resolution. Short laser pulses contribute to good temporal resolution on the order of 10–30 ns. When a resonance transition is pumped, DFWM produces a relatively strong signal. The arrangement of the three laser beams requires that the signal beam be a phase conjugate of the probe beam. This coherent signal allows for maximum signal collection and stray light rejection. DFWM also has the advantage of requiring a single laser, and optical access is minimal since the signal produced is a conjugate beam.

Although all of the groundwork for DFWM was laid down by the late 1970s, it has not been until recently that DFWM has been widely recognized as a method for sensitive measurement of absorbing species concentrations. Pender and Hesselink [23] first demonstrated DFWM in flames by measuring sodium in a seeded flame. The DFWM method has been successfully used to monitor small concentration levels of OH and NH in atmospheric flames [24], NO in flames [25, 26] and NO₂ in flames and cells [27–29].

To the authors’ knowledge, there have been no previous smoke measurements by DFWM.

In this study, the sensitivity and dynamic range of the DFWM method for measuring smoke is determined from measurements in a sample cell. Since both smoke and NO₂ absorb broadly in the visible, the performance of the DFWM system is first determined for NO₂ gas that is easier to control and vary. Laser saturation effects were investigated and found to be important at high laser energy levels. The signal beam dependence on concentration for NO₂ and smoke was determined. Single-pulse DFWM measurements were made

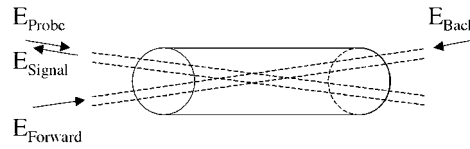


Figure 1. A typical degenerate DFWM configuration crossing in a sample cell.

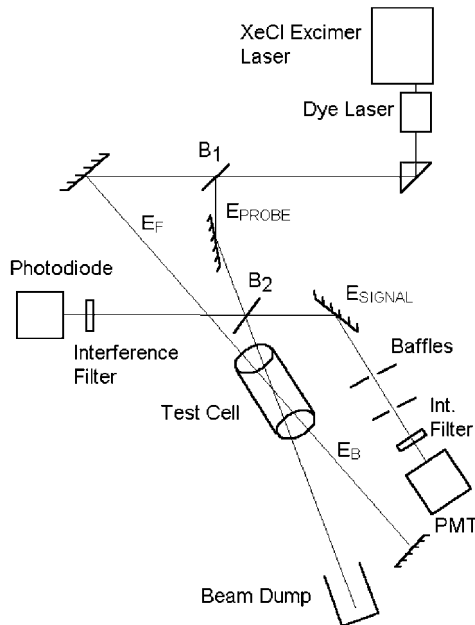


Figure 2. Schematic diagram of the DFWM system.

in sample cells over a wide concentration range to estimate the accuracy of time- and spatially resolved *in situ* measurements.

2. Experimental setup

DFWM is a nonlinear process in which three laser beams of the same frequency interact to form a fourth, phase conjugate beam. Figure 1 shows the direction and orientation of the three beams. The forward and backward pump beams, E_f and E_b , have approximately equal magnitudes and travel in opposing directions. A third beam E_{probe} enters the crossing region at a small angle to the first two beams. The interference between each pair of beams produces a Bragg grating, and the remaining beam interacts with this grating. Although part of this beam may continue through the crossing region, part of the light scatters off the grating and forms the fourth beam E_{signal} . Conservation of energy requires that this fourth beam have the same frequency as the other beams, and conservation of momentum constrains the fourth beam to travel in the opposite direction of E_{probe} .

The experimental apparatus used in this work is shown in figure 2. The Lumonics HyperEx-400 XeCl excimer laser produces a 30 ns laser pulse and operates at 308 nm. This was used to pump a Lumonics HyperDye-300 dye laser, which had a final beam size of $\approx 1.2 \text{ mm} \times 2.4 \text{ mm}$ and a pulse length of about 20 ns. Typical energy output levels were 3.0 mJ/pulse for the NO₂ work and 2.2 mJ/pulse for the smoke measurements. The wavelength of the dye laser was set to 500 nm. Both

NO_2 and smoke have broad absorption profiles that span the visible spectrum and the choice of laser wavelength is not critical. In the previous NO_2 measurements, DFWM signals were obtained from a doubled YAG laser at 532 nm [27, 29] and from dye lasers at 450–480 nm [27], 558–572 nm [28], and 563–577 nm [29].

As seen in figure 2, the light beam from the dye laser was directed through a prism and into a 50/50 beamsplitter (B_1). Half of the beam continued through the beamsplitter and a mirror directed it into the sample cell to form E_f . Upon exiting the sample cell this beam was directed back onto itself by another mirror to form E_b . The light that is reflected off the beamsplitter (B_1) travels through a second beamsplitter (B_2) and enters the sample cell at an angle of approximately 4° to E_f . This beam forms the third beam E_{probe} , and is deposited in a beam dump after leaving the cell. The signal beam, E_{signal} , exits the cell along the same path that E_{probe} entered the cell. The signal is removed by the second beamsplitter (B_2) and is directed through a series of apertures and baffles toward the photomultiplier tube (PMT) used to measure its intensity. An interference filter (Oriel no 57161) having maximum transmittance at 508.5 nm (10 nm bandwidth) is located in front of the PMT to block out stray room light. The laser pulse energy was monitored by a photodiode, which received the portion of E_{probe} reflected off the second beamsplitter. An interference filter (Oriel no 59345, 510 nm peak transmittance, 10 nm bandwidth) having a 2% transmittance at 500 nm was placed in front of the photodiode for stray light rejection and also to guard against detector saturation. The signals from the PMT and photodiode was collected through a Stanford Research SR250 gated integrator and stored on a personal computer.

The spatial resolution of the system is related to the size of the beam crossing zone, which is $1.2 \text{ mm} \times 2.4 \text{ mm} \times 34 \text{ mm}$ based on the cross-section of the dye laser beam and beam crossing angle. The actual spatial resolution is smaller than this value since most of the signal is generated near the centre of the crossing region where the laser irradiance is the greatest. The total laser irradiance in the measurement volume was about 5 MW cm^{-2} .

The NO_2 measurements were made in a 200 mm long cylindrical sample cell having an inner diameter of 25 mm. The dilutions of NO_2 gas were made by pumping the sample cell down to ≈ 0.1 Torr and then filling the cell with the desired pressure of a calibrated mixture of 200 ppm NO_2 in nitrogen. The NO_2 was diluted by adding additional N_2 to bring the total cell pressure up to 745 Torr. The measurements were taken and usually consisted of 500 laser shots. The cell was then pumped back down to 0.1 Torr, and the process was repeated for the next NO_2 concentration. The pressure measurements of NO_2 were made using an MKS Baratron[®] gauge.

A smoke generator shown in figure 3 produces carbon particles ranging from 0.1 to $0.2 \mu\text{m}$ diameter based on TEM analysis [8]. A solution of carbon black and water travels through a nebulizer and enters a heated aluminum tube, where the water is evaporated leaving a carbon-particle-laden flow of gas. These particles enter the same sample cell as described above and exit through the exhaust. The concentration of smoke is varied by diluting the carbon black/water solution. Nitrogen is used to drive the solution through the system.

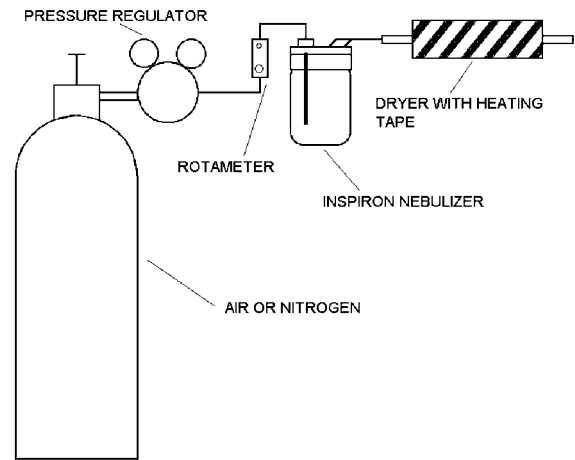


Figure 3. Schematic diagram of the smoke generator.

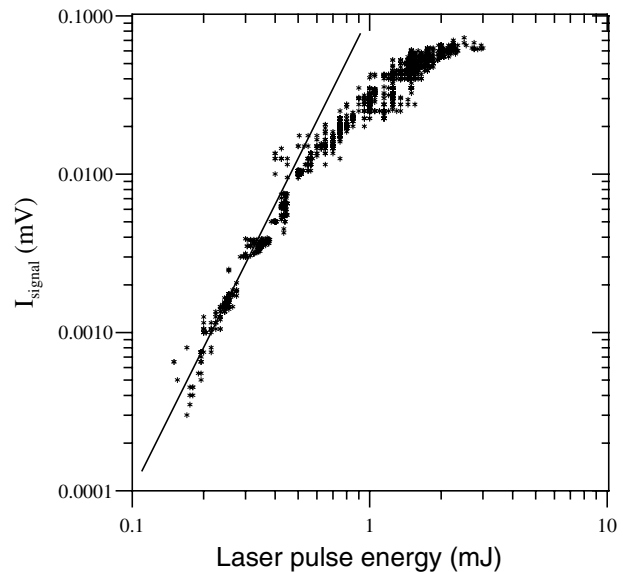


Figure 4. DFWM signal dependence on the laser pulse energy when measuring 200 ppm NO_2 in N_2 at 745 Torr pressure. The straight line is a cubic dependence.

3. Results and discussion

The dependence of I_{signal} on laser irradiance was determined by measuring NO_2 (200 ppm NO_2 in N_2 at 745 Torr absolute pressure) at several laser pulse energy levels. The resulting curve is shown in figure 4, where the DFWM signal is plotted against the measured laser pulse energy. Each data point is the DFWM signal measured for a single laser pulse. Given a fixed beam cross-section ($1.2 \text{ mm} \times 2.4 \text{ mm}$) in the measurement volume, the laser energies of 0.1–10 mJ/pulse correspond to laser irradiances of about 0.2 to 20 MW cm^{-2} . A solid line representing a cubed dependence on laser irradiance is also shown as a point of reference. Below 0.5 mJ/pulse (0.9 MW cm^{-2}), the DFWM signal followed a cubic dependence as expected from the previous measurements of NO_2 in a high-pressure (~ 700 Torr) buffer gas at low laser irradiance [27] and from a simple DFWM model of thermal gratings in a high-pressure, quenching buffer gas [30].

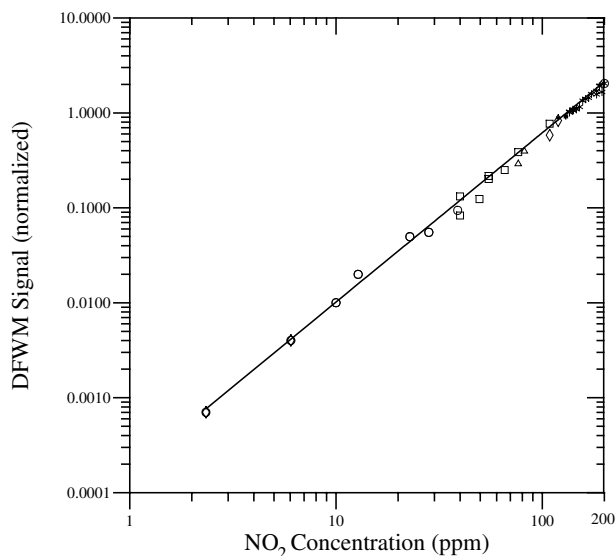


Figure 5. DFWM signals versus NO₂ concentration varying from 2.5 to 200 ppm in balance N₂ (745 Torr) in a static sample cell. Different symbols correspond to data taken on separate days. The best-fit line shown is $I_{\text{signal}} \propto N_{\text{NO}_2}^{1.9}$.

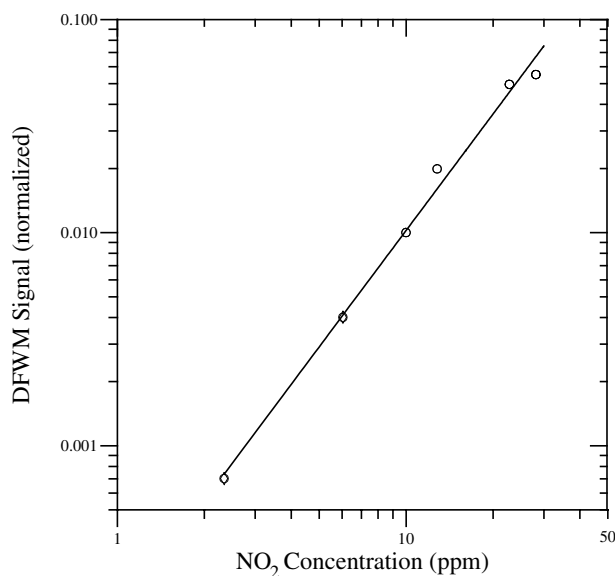


Figure 6. Expanded view of lower concentration of NO₂ data from figure 5. Different symbols correspond to data taken on separate days.

The DFWM signal levelled off for laser energy levels greater than 1.8 mJ/pulse (3 MW cm⁻²) similar to previous measurements at high laser irradiance [28]. The molecular transition is totally saturated and the signal no longer shows any dependence on laser irradiance. This region represents ideal operating conditions, since the signal is no longer sensitive to slight variations of pump irradiance. This region also creates the strongest signal, since all of the molecules in the pumped ground state are contributing to the process.

Below 1.8 mJ/pulse, the DFWM signal is increasingly dependent on laser pulse energy. This region represents an area in which the DFWM signal's dependence on laser energy varies greatly over different laser pulse energy ranges. For the

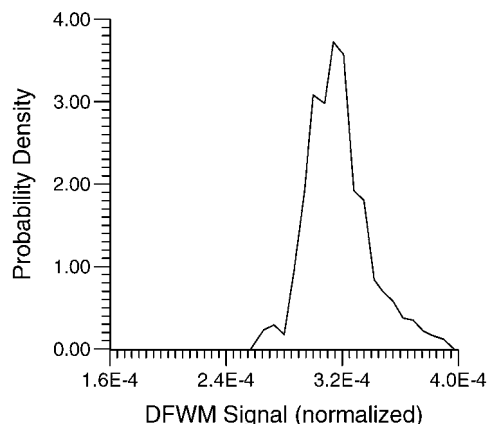


Figure 7. Probability density function of 500 single-shot DFWM measurements of 2.5 ppm concentration of NO₂ in N₂ (745 Torr). The relative standard deviation is 8.3%.

NO₂ measurements, to properly normalize the DFWM signals for laser pulse energy, the curve in figure 4 was fitted by a series of equations following the general form $I_{\text{signal}} \propto (I_{\text{laser}})^n$ where the exponent, n , was determined over a small laser pulse energy range. At high laser pulse energy, the value of n was zero indicating no dependence on laser pulse energy. Once these various laser pulse energy ranges of the curve were fitted, the DFWM signals were normalized for laser pulse energy variation according to the local value of the exponent, n .

The resulting normalized NO₂ data is presented in figure 5. The equation of the best-fit line shown in this figure has the form

$$I_{\text{signal}} \propto N_{\text{NO}_2}^{1.9} \quad (1)$$

This agrees quite well with the squared dependence on concentration found in a simple DFWM model of thermal gratings in a high-pressure, quenching buffer gas [30]. An expanded view of the lower concentration levels with the same best-fit curve is shown in figure 6. The data correlate remarkably well with the best-fit curve, even at the lower concentration levels. The level of background noise was 14% of the lowest recorded signal, and was therefore within acceptable limits. A probability density function for the lowest concentration measurement (2.5 ppm) is shown in figure 7. The 500 laser shots averaged for this point showed a standard deviation of 8.3%, which was a typical value for this set of data.

DFWM measurement of smoke concentration is shown in figures 8 and 9. The DFWM signal was not normalized for dependence on laser irradiance. However, the dye laser output pulse energy averaged 2.2 mJ/pulse and was constant to within $\pm 3\%$. Figure 8 shows a range of smoke concentrations (0.1–10 mg m⁻³) typically found in the exhausts of jet engines. Each point represents an average of 500 laser shots. The error bars represent the standard deviation of the 500 points. Overall there is good agreement between the data and the best-fit line seen in figures 8 and 9, which is of the form

$$I_{\text{signal}} \propto N_{\text{soot}}^{1.8} \quad (2)$$

As with NO₂, the smoke signal dependence on concentration agrees fairly well with the squared dependence of a simple

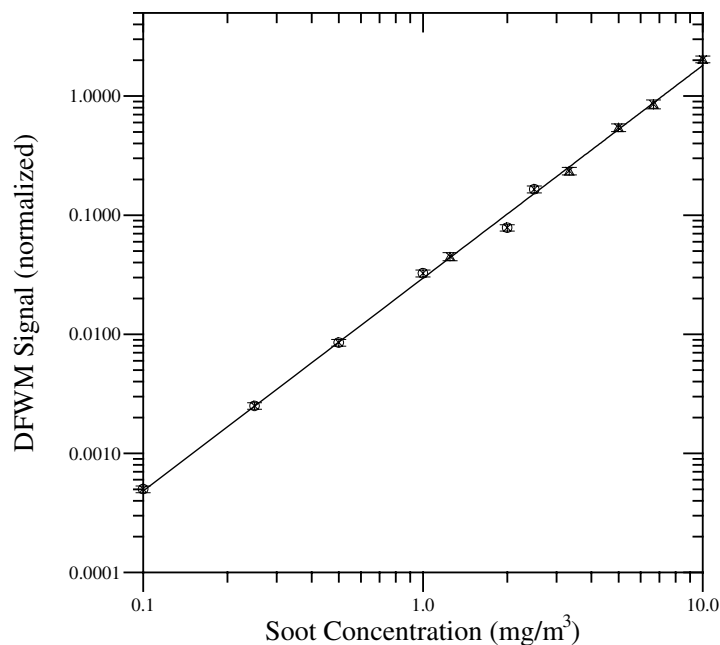


Figure 8. DFWM signals versus soot concentration varying from 0.1 to 10 mg m⁻³ (soot volume fractions ranging from 0.1 to 10 ppb) diluted in N₂ in a flowing sample cell at room pressure (760 Torr). Different symbols correspond to data taken on separate days. The average power level of these measurements was 2.2 mJ/pulse. The best-fit line shown is $I_{\text{signal}} \propto N_{\text{soot}}^{1.8}$.

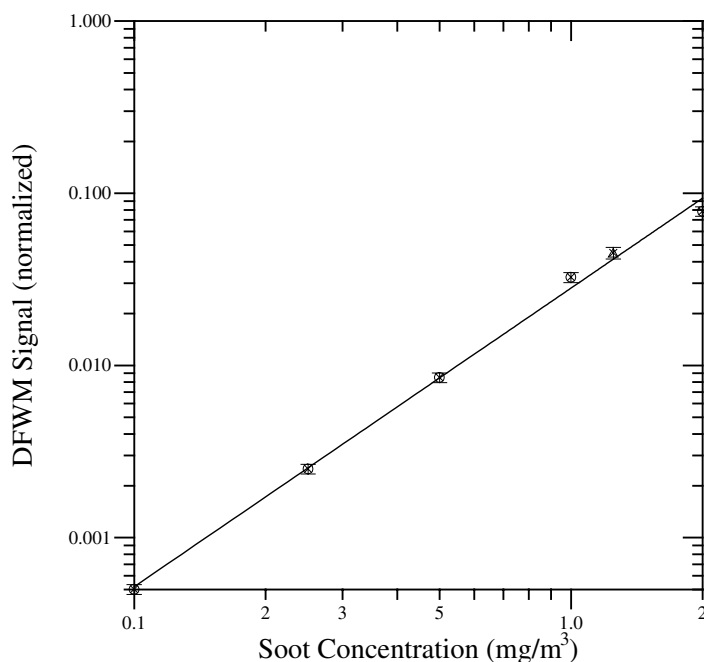


Figure 9. Expanded view of lower concentration of soot data from figure 8. Different symbols correspond to data taken on separate days.

DFWM model of thermal gratings in a high-pressure, quenching buffer gas [30].

The DFWM signal seen in figure 8 is probably enhanced by vaporization of the smoke particles by the intense laser beam. Although the laser irradiance used here ($\sim 3 \text{ MW cm}^{-2}$) is below values used to vaporize soot in the LII method [15, 16], soot vaporization has been observed in previous work for similar levels of laser irradiance [8]. Vaporization during the laser pulse increases the rate of energy transfer to the buffer gas. In addition, if C₂ molecules are formed, several lines

of the C₂ Swan bands could be resonantly pumped around 500 nm [31]. Thus the choice of 500 nm excitation could have led to stronger DFWM signals in this work from resonant pumping of laser-produced C₂.

A probability density function for the 0.25 mg m⁻³ soot measurement is shown in figure 10. This is a soot volume fraction of about 0.2 ppb and shows the excellent sensitivity of the DFWM method measuring soot. A 7.9% standard deviation occurred over this measurement, which was a typical value for the entire range of measurements.

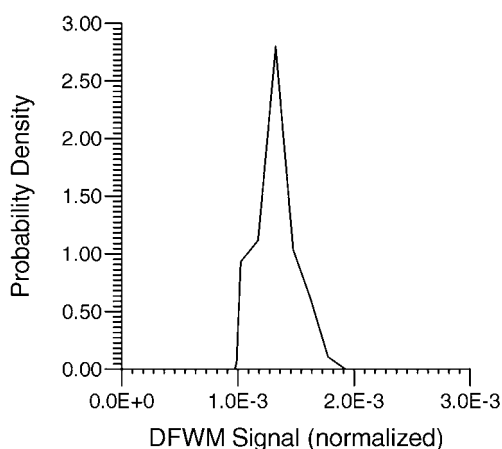


Figure 10. Probability density function of 500 single-shot DFWM measurements of 0.25 mg m^{-3} concentration of soot (a soot volume fraction of 0.25 ppb) in nitrogen (760 Torr). The relative standard deviation is 7.9%.

In this work, the standard deviations were relatively constant over the entire range of smoke and NO_2 concentration levels, suggesting that the fluctuations are due to effects other than shot noise from low signal levels. The signal variation may be a result of pulse-to-pulse variations of the dye laser (e.g. pointing instabilities, mode fluctuations). A reference beam system similar to that used in CARS systems [32] would decrease DFWM fluctuations derived from the dye laser.

4. Conclusions

As a laser diagnostic technique, DFWM has been shown to be capable of monitoring a wide range of NO_2 (2–200 ppm) and smoke ($0.1\text{--}10 \text{ mg m}^{-3}$) concentrations within a sample cell environment. The DFWM is very sensitive measuring low levels of NO_2 (2 ppm) and smoke (0.1 mg m^{-3} or 0.1 ppb soot volume fraction). Below saturation levels, the DFWM signal from NO_2 varies as the cube of the laser irradiance as expected. Above saturation, the NO_2 signal showed no laser irradiance dependence. The NO_2 and smoke signals vary nearly as the square of the concentration following a simple DFWM model of thermal gratings formed in a high-pressure, quenching buffer gas [30]. Single-pulse measurements in cells over a wide range of NO_2 and smoke levels indicate that time- and space-resolved *in situ* measurements are feasible in engine exhausts.

Acknowledgments

The authors are grateful to the National Science Foundation (PVI grant CTS-8657130) and Tennessee Space Grant Consortium for supporting this work. RWP wishes to thank Dr Michael Brown at ISSI, Inc. in Dayton, OH for his helpful comments.

References

- [1] Seinfeld J H and Pandis S N 1998 *Atmospheric Chemistry and Physics: from Air Pollution to Climate Change* (New York: Wiley)
- [2] Finlayson-Pitts B J and Pitts J N Jr 1997 Tropospheric air pollution: ozone, airborne toxics, polycyclic aromatic hydrocarbons, and particles *Science* **276** 1045–52
- [3] Shaffernocker W M and Stanforth C M 1968 Smoke measurement techniques *SAE Paper* 680346 (Warrendale, PA: Society of Automotive Engineers)
- [4] Aerospace Recommended Practice 1997 *Aircraft Gas Turbine Engine Exhaust Smoke Measurement ARP 1179C* (Warrendale, PA: Society of Automotive Engineers) (revised October)
- [5] Faxvog F R and Roessler D M 1979 Optoacoustic measurements of diesel particulate emissions *J. Appl. Phys.* **50** 7880–2
- [6] Japar S M and Szkarlat A C 1981 Measurement of diesel vehicle exhaust particulate using photoacoustic spectroscopy *Combust. Sci. Tech.* **24** 215–9
- [7] Pitz R W 1990 Low level smoke emission measurements from a flame by photothermal deflection spectroscopy *Appl. Opt.* **29** 2418–23
- [8] Brown T M, Pitz R W, Hess C F and Wood C P 1994 Pulsed photothermal laser deflection for low-level smoke and NO_2 measurements in engine exhausts *Appl. Phys. B* **59** 351–6
- [9] Rose A and Gupta R 1986 Application of photothermal and photoacoustic deflection techniques to sooting flames; velocity, temperature, and concentration measurements *Opt. Commun.* **56** 303–8
- [10] Eckbreth A C 1977 Effects of laser-modulated particulate incandescence on Raman scattering diagnostics *J. Appl. Phys.* **48** 4473–9
- [11] Melton L A 1984 Soot diagnostics based on laser heating *Appl. Opt.* **23** 2201–8
- [12] Dec J E, zur Loye A O and Siebers D L 1991 Soot distribution in a D. I. diesel engine using 2-D laser-induced incandescence imaging *SAE Paper* 910224 (Warrendale, PA: Society of Automotive Engineers)
- [13] Dec J E 1992 Soot distribution in a D. I. diesel engine using 2-D imaging of laser-induced incandescence, elastic scattering, and flame luminosity *SAE Paper* 920115 (Warrendale, PA: Society of Automotive Engineers)
- [14] Tait N P and Greenhalgh D A 1993 PLIF imaging of fuel fraction in practical devices and LII imaging of soot *Ber. Bunsenges. Phys. Chem.* **97** 1619–25
- [15] Quay B, Lee T-W, Ni T and Santoro R J 1994 Spatially resolved measurements of soot volume fraction using laser-induced incandescence *Combust. Flame* **97** 384–92
- [16] Vander Wal R L and Weiland K J 1994 Laser-induced incandescence: development and characterization towards a measurement of soot-volume fraction *Appl. Phys. B* **59** 445–52
- [17] Vander Wal R L, Zhou Z and Choi M Y 1996 Laser-induced incandescence calibration via gravimetric sampling *Combust. Flame* **105** 462–70
- [18] Shaddix C R and Smyth K C 1996 Laser-induced incandescence measurements of soot production in steady and flickering methane, propane, and ethylene diffusion flames *Combust. Flame* **107** 418–52
- [19] Pitz R W 1986 Advanced optical smoke meters for jet engine exhaust measurement *NASA Report* CR-179459
- [20] Case M E and Hofeldt D L 1996 Soot mass concentrations measurements in diesel engine exhaust using laser-induced incandescence *Aerosol Sci. Technol.* **25** 46–60
- [21] Wainner R T, Seitzman J M and Martin S R 1999 Soot measurements in a simulated engine exhaust using laser-induced incandescence *AIAA J.* **37** 738–43
- [22] Schäfer K *et al* 2000 Nonintrusive optical measurements of aircraft engine exhaust emissions and comparison with standard intrusive techniques *Appl. Opt.* **39** 441–55
- [23] Pender J and Hesselink L 1985 Phase conjugation in a flame *Opt. Lett.* **10** 264–6
- [24] Dreier T and Rakestraw D J 1990 Degenerate four-wave mixing diagnostics on OH and NH radicals in flames *Appl. Phys. B* **50** 479–85

- [25] Farrow R L and Rakestraw D J 1992 Detection of trace molecular species using degenerate four-wave mixing *Science* **257** 1894–900
- [26] Vander Wal R L, Farrow R L and Rakestraw D J 1992 High-resolution investigation of degenerate four-wave mixing in the γ (0,0) band of nitric oxide *Proc. Combust. Inst.* **24** 1653–9
- [27] Mann B A, O’Leary S V, Astill A G and Greenhalgh D A 1992 Degenerate four-wave mixing in nitrogen dioxide: application to combustion diagnostics *Appl. Phys. B* **54** 271–7
- [28] Garman J D and Dunn-Rankin D 1993 Dependence of NO₂ degenerate four-wave mixing signals on buffer gas pressure *SPIE Proc.* **1862** 133–40
- [29] Smith A P, Hall G, Whitaker B J, Astill A G, Neyer D W and Delve P A 1995 Effects of inert gases on the degenerate four-wave mixing spectrum of NO₂ *Appl. Phys. B* **60** 11–18
- [30] Danehy P M, Paul P H and Farrow R L 1995 Thermal-grating contributions to degenerate four-wave mixing in nitric oxide *J. Opt. Soc. Am. B* **12** 1564–76
- [31] Phillips J G and Davis S P 1968 *The Swann System of the C₂ Molecule: the Spectrum of the HgH Molecule* (Berkeley, CA: University of California Press)
- [32] Eckbreth A C 1996 *Laser Diagnostics for Combustion Temperature and Species* (Amsterdam: Gordon and Breach)